

Adaptive Robust Optimization with Data-Driven Uncertainty for Enhancing Distribution System Resilience

Shuyi Chen, Shixiang Zhu, Ramteen Sioshansi

Abstract—Extreme weather events are placing growing strain on electric power systems, exposing the limitations of purely reactive responses and prompting the need for proactive resilience planning. However, existing approaches often rely on simplified uncertainty models and decouple proactive and reactive decisions, overlooking their critical interdependence. This paper proposes a novel tri-level optimization framework that integrates proactive infrastructure investment, adversarial modeling of spatio-temporal disruptions, and adaptive reactive response. We construct high-probability, distribution-free uncertainty sets using conformal prediction to capture complex and data-scarce outage patterns. To solve the resulting nested decision problem, we derive a bi-level reformulation via strong duality and develop a scalable Benders decomposition algorithm. Experiments on both real and synthetic data demonstrate that our approach consistently outperforms conventional robust and two-stage methods, achieving lower worst-case losses and more efficient resource allocation, especially under tight operational constraints and large-scale uncertainty.

Index Terms—Power grid resilience, proactive planning, robust optimization, conformal prediction.

I. INTRODUCTION

The frequency and severity of extreme weather events have increased dramatically in recent years, placing unprecedented stress on electric power systems [1], [2]. For example, in March 2018, when the northeastern United States was hit by three winter storms in just 14 days, power failures across the New England region affected more than 2,755,000 customers, causing total economic losses of \$4 billion, including \$2.9 billion in insured losses [3]. These events underscore the growing vulnerability of modern power grids and highlight the urgent need for resilient grid planning that can both withstand and recover from large-scale disruptions [2], [4]–[7].

Most existing efforts in the literature and practice have focused on developing *reactive* strategies – actions taken during or after an outage to restore functionality [8]. These include dispatching emergency repair crews [9], deploying mobile backup units [10], and rerouting electricity through alternate paths [11]. While critical for mitigating immediate impacts, reactive responses are often hampered by access constraints, limited resources, and response delays. In severe cases, such as downed transmission lines or damaged substations, restoration may be impossible in the short term, rendering reactive measures insufficient to fully recover system functionality [12].

As a result, there is growing recognition of the need for *proactive* resilience strategies – interventions taken *before* extreme events occur – to reduce risk and mitigate long-term consequences [8], [12]–[15]. Such strategies include hardening infrastructure, undergrounding lines in high-risk

regions, enhancing insulation, expanding vegetation clearance, and pre-positioning recovery crews [16], [17]. Effective planning requires forecasting not only where extreme weather may strike but also the magnitude of its potential impact, and coordinating both long-term investments (*e.g.*, infrastructure upgrades) and short-term operational responses (*e.g.*, emergency deployments).

However, many existing literature falls short in capturing the full complexity of proactive resilience planning. First, many models rely on heuristic or simplified uncertainty representations – such as fixed probability distributions, historical averages, or hand-crafted scenarios – that fail to capture the high-dimensional, spatio-temporal complexity of weather-driven disruptions and lack formal guarantees. This can lead to either overfitting to past events or under-preparation for plausible but extreme scenarios. Second, proactive and reactive decisions are frequently treated in isolation. Many models either omit reactive decisions altogether or oversimplify them, ignoring the crucial interdependencies between pre-event investments and post-event response. In reality, these decisions are tightly coupled: proactive hardening shapes the feasibility of reactive operations, while reactive capacity should influence where proactive investments are made. Ignoring this interdependence can yield infeasible or suboptimal strategies under stress.

Addressing these limitations introduces three core methodological challenges: *(i) Complexity of risk modeling*: The impacts of extreme events vary drastically across space and time. Their nonstationary and high-dimensional nature makes them poorly suited for traditional parametric or distribution-based models [18]–[20]. *(ii) Data scarcity*: Extreme weather events are rare and regionally imbalanced, with limited historical records that are often noisy and sparse [6]. These limitations render standard statistical learning techniques unreliable and call for distribution-free or data-efficient alternatives. *(iii) Optimization under nested decision structures*: The interaction between uncertain events, reactive operational decisions, and proactive infrastructure investments forms a deeply nested decision-making problem. Unlike standard robust or stochastic optimization, the objective function in this setting jointly depends on decisions made before and after uncertainty is realized. This entanglement invalidates conventional decomposition techniques and complicates tractable reformulation.

To address the above challenges, we propose a novel tri-level optimization framework that explicitly models the interactions between proactive protection, uncertain disruptions, and reactive response, as demonstrated in Fig. 1. At the outer level, the model selects proactive investments (*e.g.*, infrastructure hardening) under a capital budget. The middle layer captures adversarial outage scenarios drawn from a high-

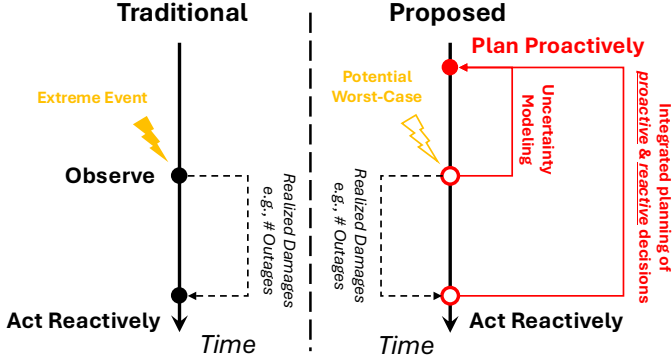


Fig. 1. Comparison between traditional reactive strategies and our proposed proactive framework. Reactive approaches respond to damage after extreme events (e.g., dispatching repair crews). In contrast, our framework plans preemptively by anticipating worst-case damages and corresponding reactive responses before events occur.

probability uncertainty set constructed via spatio-temporal conformal prediction [16], [20], which provides distribution-free coverage guarantees using finite samples. The inner layer models the reactive dispatch of recovery resources, constrained by operational budgets and infrastructure availability. To solve this complex tri-level problem, we first reformulate it into a bi-level program by applying strong duality to the inner linear program. We then apply Benders decomposition algorithm [21] that iteratively solves a master problem over proactive decisions and a subproblem that computes the worst-case damage under reactive response. This decomposition enables an efficient solution even for large-scale power systems with hundreds of regions and tight resource constraints.

We validate our approach through comprehensive experiments using both synthetic grid environments and real-world outage data from U.S. utilities. In synthetic instances, we systematically vary problem size, noise levels, and budget constraints to examine robustness and scalability. In real data, we used Massachusetts county-level weather and outage information to evaluate the effectiveness of proactive action [22], [23]. Our results reveal three key insights. First, jointly optimizing proactive and reactive decisions yields significantly lower worst-case losses compared to traditional approaches that treat them separately. This benefit is especially pronounced in resource-limited settings. Second, conformal prediction-based uncertainty sets enhance robustness by adapting to spatial heterogeneity, though their advantage diminishes in high-noise regimes where predictive intervals widen. Third, the proposed decomposition-based algorithm achieves near-optimal solutions while scaling efficiently to problem sizes, making it suitable for operational use in resilience planning.

In sum, this paper makes the following key contributions:

- 1) We introduce a tri-level decision framework that jointly optimizes proactive and reactive grid resilience actions under uncertainty.
- 2) We develop a spatio-temporal conformal prediction method to construct data-driven and distribution-free uncertainty sets for modeling extreme weather-induced outages.
- 3) We propose a novel Benders decomposition algorithm to solve the resulting bi-level optimization efficiently.

- 4) We validate the effectiveness of the proposed framework through extensive synthetic and real-world experiments, demonstrating its practical value and robustness.

The remainder of this paper is organized as follows. Section II reviews prior work on grid resilience, robust optimization, and conformal prediction. Section III details the tri-level optimization formulation and uncertainty modeling. Section IV describes our solution strategy based on duality and Benders decomposition. Section V validates the approach on synthetic data, while Section VI applies it to a real-world case study. Section VII concludes with key insights and future directions.

II. RELATED WORK

This section surveys key methodological foundations for power grid resilience planning under uncertainty. We organize the discussion into two major areas: (i) robust optimization (RO) and its extensions, including adaptive robust optimization (ARO), decision-dependent uncertainty (DDU), and tri-level optimization frameworks; (ii) spatio-temporal models for outage prediction and conformal prediction methods for uncertainty quantification in power systems.

Robust Optimization for Grid Resilience. Grid resilience refers to the ability of power systems to withstand and recover from disruptive events such as extreme weather or cyber-physical attacks [2], [10]. Robust Optimization (RO) has been a foundational tool for resilience planning, offering worst-case performance guarantees through set-based uncertainty modeling [24]. RO has been widely applied to optimize infrastructure hardening and network investments against worst-case disruptions. For instance, [25] develops a single-stage RO model for transmission expansion under uncertain renewable generation and load, ensuring feasibility across all scenarios in a predefined uncertainty set without relying on recourse actions. However, this approach lacks adaptivity and treats disruption-response planning as static, in contrast to our tri-level framework which explicitly models sequential interactions between proactive decisions, realized disruptions, and reactive responses.

While RO ensures robustness, it can become overly conservative, especially in high-dimensional or heterogeneous uncertainty settings [26]–[28]. Adaptive Robust Optimization (ARO) mitigates this by allowing recourse decisions to adapt after observing uncertainty. [26] proposes affine decision rules to improve tractability, and [29] introduces K -adaptability, where a finite set of second-stage policies is pre-optimized. ARO has been applied in unit commitment [30], economic dispatch, and outage restoration. [19] proposes the column-and-constraint generation (CCG) method for scalable ARO solutions, extended by [31] to resilience planning under both short-term and long-term uncertainties. While ARO captures decision adaptivity, it typically assumes a separable objective structure for tractability. Our proposed tri-level formulation generalizes this setting by modeling proactive decision and reactive recovery within a unified optimization framework.

Recent works on Decision-Dependent Uncertainty (DDU) explore settings where decisions influence the structure of uncertainty, such as when infrastructure upgrades reduce future

disruption risks [32]. [33] extends the CCG method to two-stage problems with DDU, enabling feedback between decision variables and uncertainty realizations. Our work differs by incorporating DDU within a tri-level structure that accounts not only for endogeneity of uncertainty but also for downstream adaptivity and budgeted responses, capturing a more realistic planning-decision loop.

A large body of tri-level optimization models such as the defender–attacker–defender (DAD) framework [34] has also been used in infrastructure protection, modeling sequential interactions between a defender’s investment, an attacker’s worst-case disruption, and a subsequent defensive response. Recent work has applied DAD framework in power system resilience modeling [8], [13]–[15], primarily under worst-case disruption scenarios. These models typically assume that hardened assets are removed from the attacker’s feasible set, thereby simplifying the interaction between proactive and reactive measures. For instance, in [8], the model excludes hardened transmission lines from the attacker’s options, effectively eliminating them from potential disruption scenarios. Moreover, these works generally rely on combinatorial or polyhedral uncertainty sets with deterministic attack budgets or spatial limits [13], [14]. Our framework differs in two key respects. First, we focus on natural hazards rather than a strategic adversary, allowing protected assets to still be affected after hardening. This reflects a more realistic interaction between proactive infrastructure investment and natural disruptions. Second, we construct localized, spatio-temporal uncertainty regions using conformal prediction informed by meteorological and demographic features. This provides finite-sample coverage guarantees and heterogeneous, region-specific risk bounds that enhance the reliability of uncertainty set estimation compared to traditional methods.

Uncertainty Modeling for Power Grid. A rich body of work has focused on modeling and forecasting power outages [35], [36]. For example, [37] use Poisson processes to model outage dynamics, while [6] apply neural networks to capture cumulative weather effects. To better represent spatial dependencies and cascading failures, graph-based approaches have been developed [17], leveraging grid topology to model outage propagation. However, most prediction-focused methods rely on assumptions like stationarity or specific parametric distributions, which may not hold in real-world scenarios, especially under rare and extreme weather conditions [16], [38], [39].

More recently, conformal prediction (CP) has gained traction for uncertainty quantification in outage modeling. CP provides distribution-free prediction sets with finite-sample coverage guarantees [18]. To address non-stationarity from extreme weather, [16], [39] introduce graph-based CP frameworks tailored to power systems. However, standard CP assumes homoskedastic noise, limiting its effectiveness in heteroskedastic settings. Normalized Conformal Prediction (NCP) [40], [41] addresses this by scaling residuals with local variability. Building on this, [20] propose a contextual conformal robust framework that integrates NCP with robust optimization to support distribution-free, context-aware decision-making. Recent extensions of NCP to spatio-temporal domains

enable both localized and system-wide uncertainty sets [39], enhancing the reliability of outage forecasting pipelines. Our work builds on these advances by embedding NCP into a decision-centric tri-level optimization framework, enabling targeted and resilient planning under heteroskedastic, weather-driven uncertainty. This integration supports robust decision-making by accounting for the variability and uncertainty inherent in power systems, especially during extreme weather events. Moreover, the distribution-free nature of conformal prediction ensures that the optimization model remains valid even when the underlying data distributions are unknown or non-stationary – conditions that frequently arise in real-world power systems facing unpredictable extreme weather [20].

III. PROPOSED FRAMEWORK

This section introduces a robust optimization framework designed to enhance power grid resilience against extreme weather events by explicitly modeling the sequential nature of decision-making under uncertainty. We propose a tri-level formulation that captures the key stages of utility planning and response, integrating long-term investment decisions, probabilistic modeling of disruptions, and real-time operational adjustments within a unified framework, as illustrated in Fig. 1. The decision process unfolds across three stages, each reflecting a distinct phase in resilience planning:

- 1) The utility first makes *proactive decisions* – such as infrastructure upgrades (e.g., pole hardening, undergrounding) or pre-positioning of repair crews – based solely on forecasts and historical data, without knowledge of the exact nature or location of the impending disruption. These early actions aim to reduce the potential impact of future outages.
- 2) Once the proactive plan is made, nature “reveals” a realization of the disruption. Here, the *uncertainty in weather-induced disruptions* is modeled adversarially: nature selects a worst-case scenario from a data-driven uncertainty set that captures plausible damage patterns, such as regional outage magnitudes. This stage formalizes the risk exposure that the proactive plan must guard against.
- 3) Lastly, the utility makes *reactive decisions* in response to the observed damage, such as dispatching crews for repair or reconfiguring the network to restore service. These decisions are constrained by available resources and must be made quickly to minimize further loss.

By structuring the model in this tri-level manner, we mirror the real-world planning cycle where proactive investments are made under uncertainty, disruptions are realized in potentially adverse ways, and recovery operations are deployed with limited capacity. This formulation allows us to optimize anticipatory actions while accounting for the worst-case outcomes and ensuring adaptive responsiveness, leading to more resilient and cost-effective grid operations under uncertainty. The notations defined in this section are summarized in Table I.

A. Problem Setup

Consider a power grid composed of n geographical regions (e.g., cities), each subject to potential outages from extreme weather events. Proactive decisions are encoded as

TABLE I
SUMMARY OF NOTATIONS

Notation	Definition
n	Number of geographical regions in the system
$\mathbf{x} = (x_i)_{i=1}^n$	$x_i = 1$ if region i is proactively protected
$\mathbf{y} = (y_i)_{i=1}^n$	$y_i = 1$ if region i receives reactive measures
$\mathbf{u} = (u_i)_{i=1}^n$	$u_i \geq 0$ indicates the number of outages in region i
$\mathbf{w} = (w_i)_{i=1}^n$	w_i represents the contextual feature of region i
$h_i, \forall i = 1, \dots, n$	Economic loss per unit outage in region i
$b_i, \forall i = 1, \dots, n$	Cost of proactive protection in region i
$c_i, \forall i = 1, \dots, n$	Cost of reactive action in region i
B	Total budget for proactive measures
C	Total budget for reactive measures
$\mathcal{U}(\mathbf{w})$	Data-driven uncertainty set for \mathbf{u} given \mathbf{w}
$[\mathcal{L}_i(\mathbf{w}), \mathcal{T}_i(\mathbf{w})]$	Local conformal prediction interval for u_i
$[\mathcal{L}_0(\mathbf{w}), \mathcal{T}_0(\mathbf{w})]$	System-level conformal interval for $\sum_i u_i$
α_0	System-wide miscoverage level
$\alpha_i, \forall i = 1, \dots, n$	Region-specific miscoverage level

$\mathbf{x} \in \{0, 1\}^n$, where $x_i = 1$ indicates region i is proactively protected. The outage magnitudes induced by extreme weather across all regions are modeled by a random vector $\mathbf{u} \in \mathbb{R}_+^n$. Its distribution is influenced by contextual features $\mathbf{w} = (w_1, \dots, w_n) \in \mathbb{R}^{n \times p}$, which capture p relevant local information such as historical outage records, weather features, and infrastructure vulnerability. Reactive decisions are similarly denoted by $\mathbf{y} \in \{0, 1\}^n$, where $y_i = 1$ means region i is selected for reactive measures. Let h_i be the economic loss per unit outage in region i .

Formally, the objective function in this framework is designed to minimize total damage across all regions, capturing the combined effects of outages, economic impact, and mitigation actions:

$$\min_{\mathbf{x}} \max_{\mathbf{u}} \min_{\mathbf{y}} \sum_{i=1}^n h_i u_i (1 - x_i) (1 - y_i), \quad (1)$$

$$\text{s.t. } \mathbb{P}\{\mathbf{u} \in \mathcal{U}(\mathbf{w})\} \geq 1 - \alpha, \quad (2)$$

$$\sum_{i=1}^n b_i x_i \leq B, \quad (3)$$

$$\sum_{i=1}^n c_i y_i \leq C. \quad (4)$$

Specifically, the term in (1) for each region i acts as a logical switch: damage is incurred only if region i is neither proactively protected ($x_i = 1$) nor reactively repaired ($y_i = 1$). If either a proactive or reactive decision is made for a region, the corresponding damage is effectively nullified in the objective. This multiplicative structure allows the model to prioritize protective actions in regions with high outage risk and economic cost while balancing limited resources. By summing over all regions, the objective captures the total system-level loss, and minimizing it encourages the model to strategically allocate proactive and reactive efforts where they are most effective under worst-case outage scenarios.

The above setup also includes three key constraints that reflect practical limitations and uncertainty considerations in grid resilience planning. Constraint (2) ensures that the potential outage magnitude \mathbf{u} lies within a high-probability

uncertainty set $\mathcal{U}(\mathbf{w}) \subseteq \mathbb{R}_+^n$, thereby accounting for uncertainty in outage scenarios while controlling the risk of infeasible outcomes. Constraint (3) imposes a budget limit on proactive decisions, where b_i denotes the cost of implementing a proactive protection measure in region i . The total investment across all regions must not exceed the available capital budget B , i.e., $\sum_{i=1}^n b_i x_i \leq B$. Similarly, constraint (4) enforces an operational budget constraint on reactive actions, where c_i represents the cost of deploying recovery resources (e.g., dispatching repair crews) to region i . The total reactive deployment cost is constrained by an upper limit C , ensuring feasibility via $\sum_{i=1}^n c_i y_i \leq C$. These two constraints jointly ensure that both proactive and reactive decisions are made within realistic resource and operational limits.

B. Constructing Chance Constraint via Conformal Prediction

To construct the chance constraint (2), we adopt conformal prediction [20], [40], [41] to build valid, data-driven uncertainty sets for the regional outage vector \mathbf{u} . Conformal prediction provides a flexible and model-agnostic framework for constructing prediction intervals with finite-sample coverage guarantees. Formally, given a nonconformity score and a calibration set, conformal prediction ensures that for any new instance \mathbf{w} , the true response \mathbf{u} lies within a predicted set $\mathcal{U}(\mathbf{w})$ with probability at least $1 - \alpha$, regardless of the underlying distribution. This guarantee aligns naturally with our goal of enforcing chance constraints on uncertain outage realizations in (2).

To capture both region-specific variability and system-wide uncertainty, we decompose the uncertainty set $\mathcal{U}(\mathbf{w})$ into two components. The first component imposes a local constraint for each region i , requiring the outage magnitude u_i to lie within a region-specific high-confidence interval with miscoverage rate α_i :

$$\mathbb{P}\left\{\widehat{\mathcal{L}}_i(\mathbf{w}) \leq u_i \leq \widehat{\mathcal{T}}_i(\mathbf{w})\right\} \geq 1 - \alpha_i, \quad \forall i = 1, \dots, n. \quad (5)$$

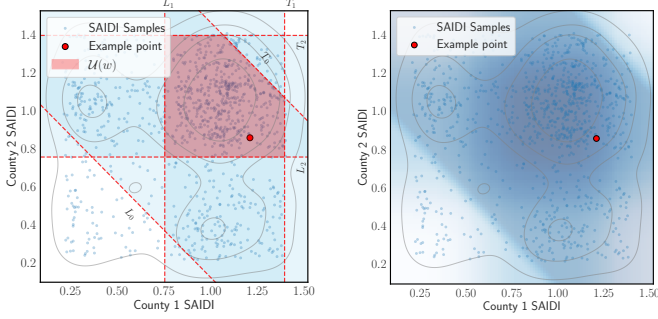
These local lower and upper estimators, $\widehat{\mathcal{L}}_i(\cdot)$ and $\widehat{\mathcal{T}}_i(\cdot)$, are derived using marginal conformal prediction, conditioned on contextual features \mathbf{w} , and are designed to reflect the heterogeneous risk profiles across different regions [20]. The second component introduces a global constraint that ensures the total system-wide outage $\sum_{i=1}^n u_i$ lies within a conformal prediction interval constructed for the aggregate with a miscoverage rate α_0 :

$$\mathbb{P}\left\{\widehat{\mathcal{L}}_0(\mathbf{w}) \leq \sum_{i=1}^n u_i \leq \widehat{\mathcal{T}}_0(\mathbf{w})\right\} \geq 1 - \alpha_0. \quad (6)$$

This global interval estimator, $\widehat{\mathcal{L}}_0(\cdot)$ and $\widehat{\mathcal{T}}_0(\cdot)$, is obtained by applying conformal calibration to the sum of predicted outages across regions, thereby capturing correlated risk structures and ensuring coherence at the system level. See Fig. 2 for an illustration of marginal and aggregated conformal bounds.

The construction of the uncertainty sets proceeds as follows:

- 1) *Data Splitting*: The available data $\{(\mathbf{w}^j, \mathbf{u}^j)\}_{j=1}^m$ collected from m historical extreme weather events is randomly partitioned into a training set and a calibration set. A



(a) Single-event Conformal Bounds (b) Empirical Conformal Bounds

Fig. 2. Data-driven uncertainty set $\mathcal{U}(\mathbf{w})$ for a two-region network under simulated outage scenarios. (a) Single-event example: marginal conformal strips $[L_1(\mathbf{w}), T_1(\mathbf{w})]$ (vertical blue bands) and $[L_2(\mathbf{w}), T_2(\mathbf{w})]$ (horizontal blue bands), the aggregated band $[L_0(\mathbf{w}), T_0(\mathbf{w})]$ (diagonal blue region), and their overlap (red shading). The red marker highlights the single-event sample, and dashed red lines show its estimated bounds. (b) Empirical coverage for all out-of-sample SAIDI pairs: overlays the marginal and aggregated conformal regions to illustrate how region-level and system-level constraints together envelop the true outage distribution. Shading intensity reflects empirical coverage across all test points. In both panels, each blue dot is a simulated SAIDI pair with gray contours for kernel density estimation of their distribution.

predictive model \hat{f} is trained on the training set to estimate the conditional mean of u_i given \mathbf{w} .

2) *Computing Nonconformity Scores*: We compute a nonconformity score for each instance in the calibration set as

$$s_i = \|u_i - \hat{f}(w_i)\|,$$

which measures the deviation between the observed and predicted values. The $(1 - \alpha_i)$ -quantile of these scores, denoted by $Q(\alpha_i)$, is used to define the local prediction interval as

$$\hat{L}_i := \hat{f}(w_i) - Q_i, \quad \hat{U}_i := \hat{f}(w_i) + Q_i.$$

A similar conformal calibration procedure is applied to the predicted total outage $\hat{f}_0(\mathbf{w}) := \sum_{i=1}^n \hat{f}(w_i)$ to derive the global prediction interval \hat{L}_0 and \hat{U}_0 .

3) *Constructing Uncertainty Set*: Combining the local and global sets, the final uncertainty set in (2) is given by:

$$\mathcal{U}(\mathbf{w}) := \left\{ \mathbf{u} : \begin{array}{l} \hat{L}_i(\mathbf{w}) \leq u_i \leq \hat{T}_i(\mathbf{w}), \quad \forall i \geq 1, \\ \hat{L}_0(\mathbf{w}) \leq \sum_i u_i \leq \hat{T}_0(\mathbf{w}). \end{array} \right\}. \quad (7)$$

This reformulation of the chance constraint in (7) yields an uncertainty set $\mathcal{U}(\mathbf{w})$ that takes the form of a convex polyhedron in \mathbb{R}^n , as illustrated by Fig. 2. This structure offers two primary advantages: (i) It provides an empirically accurate approximation of the true high-confidence region. Although the underlying uncertainty set may be non-convex or complex, the polyhedral approximation captures its essential geometry with high fidelity and interpretability; (ii) The convexity and linearity of the resulting constraints offer substantial benefits for optimization. This avoids introducing nonlinearity or combinatorial complexity, thereby preserving the tractability of the overall problem and enabling efficient solution using standard optimization solvers. In summary, the conformal prediction-based uncertainty representation not only provides reliable

Algorithm 1 Conformal Uncertainty Set Construction

Input: Data $\mathcal{D} = \{(\mathbf{w}^j, u^j)\}_{j=1}^m$, miscoverage level α ;

Output: Uncertainty set $\mathcal{U}(\mathbf{w})$;

- 1: Randomly split data \mathcal{D} into $\mathcal{D}_{\text{train}}$ and \mathcal{D}_{cal} ;
- 2: Train prediction model $\hat{f}(\mathbf{w})$ on $\mathcal{D}_{\text{train}}$;
- 3: **for** $i = 0, 1, \dots, n$ **do**
- 4: $\mathcal{S}_i \leftarrow \emptyset$;
- 5: **for** each $(w_i^j, u_i^j) \in \mathcal{D}_{\text{cal}}$ **do**
- 6: $s_i^j \leftarrow \|u_i^j - \hat{f}_i(\mathbf{w}^j)\|$;
- 7: $\mathcal{S}_i \leftarrow \mathcal{S}_i \cup \{s_i^j\}$;
- 8: **end for**
- 9: $Q_i \leftarrow (1 - \alpha)$ -quantile of \mathcal{S}_i ;
- 10: $\hat{L}_i(\mathbf{w}) \leftarrow \hat{f}_i(\mathbf{w}) - Q_i, \quad \hat{T}_i(\mathbf{w}) \leftarrow \hat{f}_i(\mathbf{w}) + Q_i$;
- 11: **end for**
- 12: Construct uncertainty set $\mathcal{U}(\mathbf{w})$ using Eq. (7)
- 13: **return** $\mathcal{U}(\mathbf{w})$

coverage guarantees but also aligns naturally with the structure of the optimization model. The overall conformal prediction procedure is summarized in Algorithm 1.

IV. SOLUTION STRATEGY

We develop an efficient and scalable solution strategy to address the computational challenges posed by the tri-level problem in (1).

The main difficulty stems from the *coupled loss function*, where the objective jointly depends on both proactive decisions \mathbf{x} and reactive decisions \mathbf{y} . This coupling invalidates standard assumptions in robust and adaptive robust optimization (RO and ARO) [26], [27], which typically rely on separability across decision stages to enable tractable reformulations [19], [31]. In addition, the uncertainty set $\mathcal{U}(\mathbf{w})$ in constraint (2) varies spatially and is defined via a high-dimensional polyhedral budget [16], [20], making direct integration into optimization layers challenging.

To address these challenges, we propose a two-step solution:

- 1) *Reformulation via Strong Duality*: We apply strong duality to the inner minimization over \mathbf{y} , transforming the tri-level problem into a bi-level structure. This reformulation embeds the reactive decision within the middle-level maximization, effectively collapsing the innermost layer.
- 2) *Benders Decomposition*: We then apply Benders decomposition to solve the resulting bi-level problem [21]. The *master problem* determines the proactive protection decisions \mathbf{x} , while the *subproblem* computes the worst-case cost by maximizing over outage vectors $\mathbf{u} \in \mathcal{U}(\mathbf{w})$, given the optimal reactive response. Benders cuts generated from the subproblem are iteratively added to the master problem to refine its feasible space.

This decomposition-based strategy improves scalability by decoupling high-level planning from worst-case evaluation, enabling efficient optimization even in large-scale power grids. For comparison, we also implement a direct reformulation using the Karush-Kuhn-Tucker (KKT) conditions (see Appendix C). As shown in Appendix D, the decomposition-based

method achieves comparable accuracy while offering superior scalability, especially for large-scale grid resilience problems.

A. Bi-level Reformulation via Strong Duality

We begin by reformulating the original tri-level problem (1) into a bi-level structure by applying strong duality to the inner minimization over the reactive decisions \mathbf{y} .

First, we relax the binary constraint on \mathbf{y} and allow the reactive decisions to be continuous. Let $\zeta_i := h_i u_i (1 - x_i)$ denote the potential economic loss in region i , given the proactive decision \mathbf{x} and outage realization \mathbf{u} . The resulting inner minimization problem seeks to reduce total loss via optimal deployment of recovery resources:

$$\min_{\mathbf{y}} \sum_{i=1}^n \zeta_i (1 - y_i), \quad \text{s.t. } y_i \in [0, 1], \quad \forall i, \quad \sum_{i=1}^n c_i y_i \leq C. \quad (8)$$

This relaxed problem is a linear program with affine constraints and a bounded feasible region. As shown in Appendix A, the relaxation preserves integrality and optimality when the reactive costs are uniform integers and the total reactive budget is also an integer. Moreover, the problem satisfies Slater's condition, guaranteeing strong duality (Appendix B). The dual of the relaxed problem is:

$$\min_{\lambda \geq 0, \mu \geq 0} \lambda C + \sum_{i=1}^n \mu_i, \quad \text{s.t. } \lambda c_i + \mu_i \geq \zeta_i, \quad \forall i, \quad (9)$$

where μ_i is the dual variable for the upper bound constraints $y_i \leq 1$. Note that we omit explicit dual variables for the lower bounds $y_i \geq 0$, as they are naturally enforced in the non-negativity domain of the primal.

We then substitute the dual in (9) back into the original tri-level objective, embedding the reactive decision layer into the adversarial maximization. The problem becomes a bi-level min-max formulation:

$$\begin{aligned} \min_{\mathbf{x}} \max_{\mathbf{u}, \lambda \geq 0, \mu \geq 0} & \sum_{i=1}^n h_i u_i (1 - x_i) - \lambda C - \sum_{i=1}^n \mu_i & (10) \\ \text{s.t. } & \lambda c_i + \mu_i \geq h_i u_i (1 - x_i), \quad \forall i, \\ & \widehat{L}_i(\mathbf{w}) \leq u_i \leq \widehat{T}_i(\mathbf{w}), \quad \forall i, \\ & \widehat{L}_0(\mathbf{w}) \leq \sum_{i=1}^n u_i \leq \widehat{T}_0(\mathbf{w}), \\ & \sum_{i=1}^n b_i x_i \leq B, \quad x_i \in \{0, 1\}. \end{aligned}$$

This bi-level formulation captures the outer optimization over proactive protections \mathbf{x} , and an inner maximization over worst-case disruptions \mathbf{u} , jointly with the optimal reactive deployment through dual variables (λ, μ) .

B. Benders Decomposition

To solve the bi-level reformulation in (10), we adopt Benders decomposition as an efficient approximation method. This approach partitions the problem into a master problem that optimizes proactive decisions \mathbf{x} , and a subproblem that evaluates the corresponding worst-case cost. The core idea is to iteratively solve a simplified master problem and refine it using cuts derived from subproblem solutions until convergence.

This approach is particularly effective for large-scale problems with convex subproblems, as is the case here. At each iteration, the algorithm updates an outer approximation of the worst-case cost function $\Phi(\mathbf{x})$, which is convex but not explicitly known. The procedure is summarized in Algorithm 2 and proceeds as follows:

- 1) *Master Problem:* The master problem selects the proactive decision \mathbf{x} and maintains an upper bound θ on the worst-case cost:

$$\min_{\theta \in \mathcal{C}, \mathbf{x}} \theta \quad \text{s.t. } x_i \in \{0, 1\}, \quad \forall i, \quad \sum_{i=1}^n b_i x_i \leq B, \quad (11)$$

where \mathcal{C} contains the accumulated Benders cuts from previous iterations.

- 2) *Subproblem:* Given a fixed \mathbf{x}^t obtained at iteration t , the subproblem evaluates the worst-case cost:

$$\begin{aligned} \Phi(\mathbf{x}^t) := \max_{\mathbf{u}, \lambda, \mu} & \sum_{i=1}^n h_i u_i (1 - x_i^t) - \lambda C - \sum_{i=1}^n \mu_i, & (12) \\ \text{s.t. } & \lambda c_i + \mu_i \geq h_i u_i (1 - x_i^t), \quad \forall i, \\ & \widehat{L}_i(\mathbf{w}) \leq u_i \leq \widehat{T}_i(\mathbf{w}), \quad \forall i, \\ & \widehat{L}_0(\mathbf{w}) \leq \sum_{i=1}^n u_i \leq \widehat{T}_0(\mathbf{w}), \\ & \mu_i \geq 0, \quad \lambda \geq 0. \end{aligned}$$

This is a convex maximization problem over the polyhedral uncertainty set $\mathcal{U}(\mathbf{w})$. The optimal value $\Phi(\mathbf{x}^t)$ provides a lower bound on the true cost for the current proactive decision \mathbf{x}^t .

- 3) *Benders Cut:* To update the master problem, we construct a supporting hyperplane (Benders' cut) to lower-bound the true worst-case cost function $\Phi(\mathbf{x})$. Since $\Phi(\mathbf{x})$ is convex in \mathbf{x} (due to pointwise maximization of affine functions), subgradients can be used to linearize it at \mathbf{x}^t . Let $\boldsymbol{\pi}^t \in \partial \Phi(\mathbf{x}^t)$ denote a subgradient, which can be obtained from the dual solution of the subproblem or computed via perturbation analysis. The Benders' cut then takes the form:

$$\theta \geq \Phi(\mathbf{x}^t) + (\boldsymbol{\pi}^t)^\top (\mathbf{x} - \mathbf{x}^t), \quad (13)$$

which ensures that the surrogate cost θ always overestimates $\Phi(\mathbf{x})$ at \mathbf{x}^t and in its neighborhood. This inequality is added to the feasible region \mathcal{C} , and improves the approximation of the true worst-case objective.

The algorithm iterates between the master and subproblem, accumulating Benders cuts until the gap between the upper bound θ from the master and the subproblem's lower bound $\Phi(\mathbf{x}^t)$ falls below a predefined tolerance ϵ . This ensures an ϵ -optimal solution to the original bi-level problem.

V. SYNTHETIC EXPERIMENT

We design a synthetic experiment with the number of cities varying from 5 to 20 to systematically assess the performance of our proposed tri-level optimization framework relative to several baseline methods under different scenarios.

Algorithm 2 Benders Decomposition for Solving (10)

Input: Tolerance ϵ ; Max iterations T ;
Output: Optimal decisions \mathbf{x}^* ;

- 1: Initialize $t \leftarrow 0$, $\mathcal{C} \leftarrow \emptyset$, $\text{UB} \leftarrow +\infty$, $\text{LB} \leftarrow -\infty$
- 2: **while** $\text{UB} - \text{LB} > \epsilon$ and $t < T$ **do**
- 3: Solve master problem in (11);
- 4: Solve subproblem $\Phi(\mathbf{x}^t)$ given fixed \mathbf{x}^t in (12);
- 5: $\text{UB} \leftarrow \min(\text{UB}, \theta^t)$; $\text{LB} \leftarrow \max(\text{LB}, \Phi(\mathbf{x}^t))$;
- 6: **if** $\Phi(\mathbf{x}^t) - \theta^t \leq \epsilon$ **then**
- 7: **break**;
- 8: **end if**
- 9: Extract dual multipliers $\boldsymbol{\pi}^t$ from subproblem;
- 10: Add Benders cut to \mathcal{C} : $\theta \geq \Phi(\mathbf{x}^t) + (\boldsymbol{\pi}^t)^\top (\mathbf{x} - \mathbf{x}^t)$;
- 11: $t \leftarrow t + 1$;
- 12: **end while**
- 13: **return** $\mathbf{x}^* \leftarrow \mathbf{x}^t$.

A. Evaluation Metrics and Baselines

To assess the robustness and adaptability of each method, we consider the following evaluation metrics: (i) *Worst-case cost*: The optimal value of the inner bi-level (max-min) problem in (1) for a given proactive decision \mathbf{x} . (ii) *Worst-case cost under local constraints only*: This variant omits the global uncertainty constraint by dropping (6), allowing disruptions to be independently bounded within each region. This is effectively the “worst-case” scenario considered in most literature, assuming the worst realization of uncertainty within the predefined set, regardless of the proactive action taken. (iii) *Worst-case cost under global constraint only*: This formulation removes all local constraints (5) and instead bounds only the total disruption across all regions via $\widehat{L}_0(\mathbf{w}) \leq \sum_i u_i \leq \widehat{T}_0(\mathbf{w})$. The third metric offers interpretability by examining how a total uncertainty “budget” is adversarially distributed across regions. Without regional limits, the most adversarial disruption allocates outages inversely proportional to cost coefficients, balancing the product of cost and disruption and discouraging excessive impact in regions where losses can be mitigated through reactive deployment. Under certain structural assumptions, this simplified model approximates the original middle-layer adversarial problem and provides insight into the nature of worst-case disruptions (see Appendix E).

Beyond worst-case evaluations, we also assess performance under empirically derived scenarios based on historical uncertainty realizations: (iv) *Mean scenario*: The outage vector is set to historical outages, and the average loss is computed on the synthetic data. (v) *1- σ and 2- σ scenarios*: Outages are scaled to one and two standard deviations above the historical mean, similarly averaged for synthetic data. These quantile-based scenarios serve as practical and interpretable stress tests for assessing robustness beyond the adversarial setting.

We compare our tri-level optimization framework with four baseline methods, representing common practical strategies: (i) *One-stage mean-based*: Proactive decisions \mathbf{x} are optimized using expected outages, without recourse. (ii) *One-stage worst-case*: Proactive decisions are optimized against the worst-case scenario within the uncertainty set $\widehat{\mathcal{U}}$, also without

TABLE II
EVALUATION OF TOTAL COST WITH SYNTHETIC DATA (UNIT: $\times 10^4$)

Method	Pred \hat{f}	Possible Realizations of $\mathbf{u} \in \mathcal{U}$			Adversarial Disruption Scheme		
		Mean Attack	1- σ	2- σ	Adv (w/o (5))	Adv (w/o (6))	Adv (with (7))
1-Stage (Mean)	Emp	/	/	/	56.94	55.15	52.06
1-Stage (Mean)	NCP	/	/	/	56.94	55.15	52.06
1-Stage (Worst)	Emp	/	/	/	56.94	55.15	52.06
1-Stage (Worst)	NCP	/	/	/	56.94	55.15	52.06
2-Stage (Mean)	Emp	49.61	55.97	62.52	53.18	53.01	49.52
2-Stage (Mean)	NCP	50.88	57.38	64.76	56.94	52.96	49.51
2-Stage (Worst)	Emp	52.07	56.79	59.91	56.94	55.15	52.06
2-Stage (Worst)	NCP	53.25	57.49	64.43	53.50	52.92	49.74
Tri-level	NCP	48.70	50.50	62.28	53.19	50.50	49.50

recourse. (iii) *Two-stage mean-based*: First-stage decisions \mathbf{x} and second-stage responses \mathbf{y} are optimized jointly using expected outages. (iv) *Two-stage worst-case*: Proactive and reactive decisions are optimized jointly for the worst-case within $\widehat{\mathcal{U}}$. While the two-stage methods allow reactive flexibility, none explicitly model adversarial uncertainty. All methods are evaluated under the same setting with $n = 10$, $B = 1000$, and $C = 1$. Mean predictions and uncertainty intervals are generated using either Normalized Conformal Prediction (NCP), which produces region-specific, heteroskedastic intervals via a neural network, or an empirical approach (Emp) based on historical data. Additional results appear in Fig.3 and AppendixD; full baseline formulations are in Appendix F.

B. Synthetic Data Generation

We generate synthetic data in two steps. First, outage trajectories for each region are simulated using a spatio-temporal SIR-style model [6], [10], [37], [42], where disruption rates respond to synthetic weather inputs exhibiting spatial and temporal correlations to mimic realistic extreme weather patterns. Disruptions are then quantified using the System Average Interruption Duration Index (SAIDI) [43], with economic weights h_i proportional to regional population N_i , reflecting that disruptions in densely populated areas incur higher costs for the same duration of downtime. This weighting aligns the objective in (1) with the real-world economic consequences by jointly capturing the scale of physical damage (u_i) and societal impact (N_i).

To model observational noise, we introduce heteroskedastic Gaussian noise to u_i , assuming the noise variance is inversely proportional to population size. This reflects the intuition that outage estimates in less populated regions are more noisy. We simulate 200 synthetic events and average results across 40 test samples. Additional details on the synthetic experiment setup are provided in Appendix G.

C. Results

Table II reports total system-level costs across various disruption scenarios. Our tri-level framework consistently outperforms one-stage and two-stage baselines, particularly under adversarial attacks, demonstrating the benefit of jointly optimizing proactive planning, uncertainty modeling, and reactive response. Notably, the tri-level framework performs well even under non-adversarial conditions, demonstrating that normalized conformal prediction (NCP) provides calibrated,

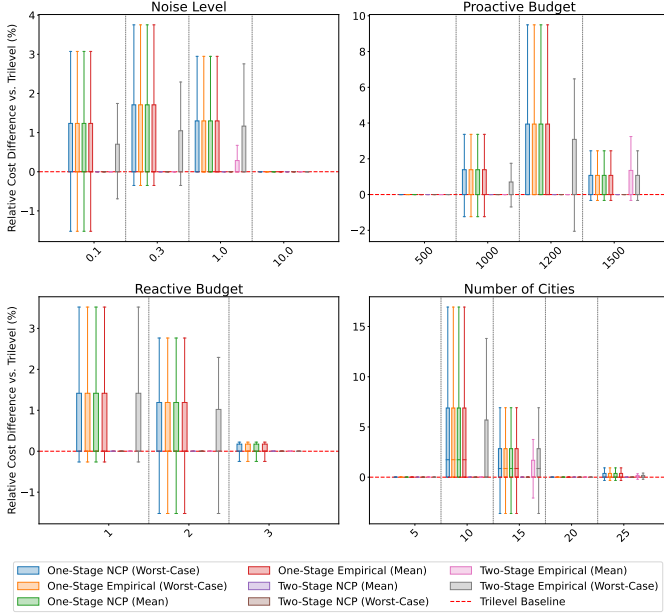


Fig. 3. Performance comparison for our method and baselines on synthetic dataset across different noise level in the generation process, proactive budget (B), reactive budget (C), and number of cities (n).

data-driven uncertainty intervals that capture heteroskedastic and region-specific variability. As a result, the model maintains strong mean-case performance across repeated runs with stochastic noise, effectively mitigating the risk of overfitting to individual point estimates. These results underscore that the method improves both robustness to extreme events and reliability in typical operating scenarios.

Fig. 3 further examines performance under varying noise levels, budgets, and system sizes. As the proactive budget increases, our model allocates resources more efficiently, widening the performance gap until all regions are protected for all methods. As the reactive budget grows, the gap diminishes monotonically, as greater post-event flexibility reduces the need for proactive planning. Under increasing noise, our method initially excels due to calibrated uncertainty bounds but loses ground as prediction intervals become overly wide and imprecise due to high noise. Importantly, as the complexity of the planning problem grows, the tri-level framework demonstrates increasing advantage. However, since the proactive budget remains fixed in our experiments—unlike in realistic settings where larger systems typically receive more resources—the marginal benefit of coordination may diminish due to limited resource, finally narrowing the performance gap.

VI. CASE STUDY

To demonstrate the practical utility of our proposed framework, we apply it to a semi-synthetic case study on power line undergrounding using real-world data from Massachusetts, provided by the local utility [6]. Undergrounding overhead distribution lines is widely recognized as a long-term strategy for enhancing grid resilience by mitigating weather-induced outages [44], [45]. However, its high cost necessitates strategic investment decisions under strict budget constraints.

TABLE III
EVALUATION OF TOTAL COST WITH MA DATA (UNIT: $\times 10^6$)

Method	Pred \hat{f}	Possible Realizations of $\mathbf{u} \in \mathcal{U}$			Adversarial Disruption Scheme		
		Third Storm	1- σ	2- σ	Adv (w/o (5))	Adv (w/o (6))	Adv (with (7))
1-Stage (Mean)	Emp	/	/	/	24.52	23.56	21.48
1-Stage (Mean)	NCP	/	/	/	24.52	23.56	21.48
1-Stage (Worst)	Emp	/	/	/	24.52	23.56	21.48
1-Stage (Worst)	NCP	/	/	/	24.52	23.56	21.48
2-Stage (Mean)	Emp	1.48	44.89	88.25	24.52	24.25	22.07
2-Stage (Mean)	NCP	<u>7.52</u>	38.84	70.22	24.52	23.56	21.48
2-Stage (Worst)	Emp	12.98	44.69	73.68	24.52	23.56	21.48
2-Stage (Worst)	NCP	20.46	58.04	96.38	23.28	22.82	<u>21.36</u>
Tri-level	NCP	19.40	58.04	96.38	23.28	<u>23.42</u>	21.13

In this study, we consider a setting where $x_i = 1$ indicates that region i is proactively protected via undergrounding, subject to the investment budget constraint (3), with b_i representing the undergrounding cost and B the total available budget. We extend our framework to a more flexible reactive-decision formulation where $y_{ij} = 1$ denotes dispatching crew j to region i . The following constraints capture operational constraints:

$$\sum_{i=1}^n \sum_{j=1}^{n'} y_{ij} \leq C, \quad \sum_{j=1}^{n'} y_{ij} \leq 1, \quad \forall i,$$

where n' is the number of available crews and C is the total number of deployable assignments. This constraint limits total deployments and ensures no region receives multiple crews.

We solve this extended tri-level optimization problem using the Benders decomposition approach. Undergrounding costs b_i are randomly sampled for each Massachusetts county as $b_i \sim \text{Unif}(100, 500)$, and all results are averaged over five independent runs to ensure robustness. All methods are evaluated under the same setting with $n = 14$, $B = 1000$, and $C = 3$. Additional details are provided in Appendix H.

A. Dataset Description

We use a real dataset comprising county-level outage counts in Massachusetts from a 2018 Nor'easter snowfall event [22], combined with meteorological data from NOAA's HRRR model [23] and socioeconomic indicators from the U.S. Census Bureau [46]. Features include wind speed, temperature, pressure, median income, age, food stamp recipients, unemployment rate, poverty rate, college enrollment, commute time, and household size—capturing both hazard intensity and social vulnerability. The dataset includes three snowstorms over a 15-day period, during which infrastructure condition is assumed unchanged. We use the first two storm for training and the third for testing. Fig. 5 (c) visualizes the spatial outage patterns.

B. Results

Table III compares the total cost under adversarial outage scenarios across methods. Our tri-level approach consistently outperforms conventional one-stage or two-stage optimization by achieving lower losses under worst-case attack. These results validate the advantage of integrating proactive investment, adversarial risk modeling, and adaptive recovery into a unified decision framework. While it does not yield the lowest cost in the specific real-world test instance, we emphasize that

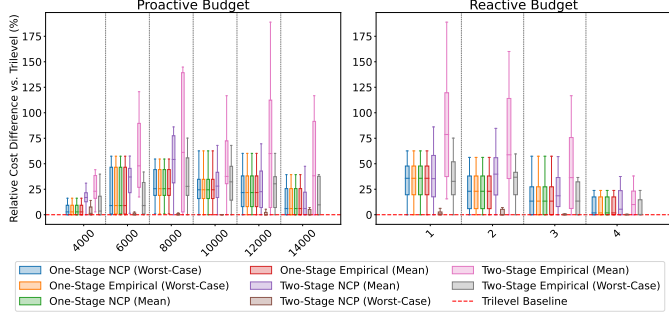


Fig. 4. Performance comparison on real-world data across different proactive (B) and reactive (C) budget levels for our method and baselines.

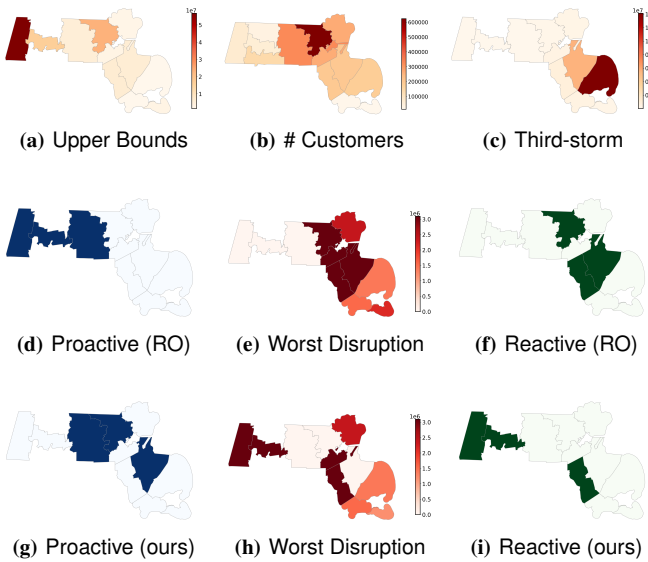


Fig. 5. Spatial distribution of SAIDI and resilience actions across Massachusetts counties under real and worst-case scenarios. (a) Upper bounds of SAIDI predicted by the NCP model weighted by number of customers. (b) Number of customers per county. (c) Actual SAIDI of the third storm weighted by number of customers. (d-f) Conventional robust-optimization (RO) model: (d) proactive undergrounding decisions, (e) induced worst-case outage disruption weighted by number of customers, and (f) optimal reactive crew dispatch. (g-i) Tri-level optimization model (ours): (g) proactive undergrounding decisions, (h) induced worst-case outage disruption weighted by number of customers, and (i) optimal reactive crew dispatch.

the first three columns in Table III reflect a single disruption instance. As such, they do not fully capture the long-term benefits of conformal prediction and its statistical properties. Furthermore, the third storm in the Massachusetts dataset was notably milder than the previous two, resulting in lower disruption levels and reduced impact proactive strategies could make [10]. Our model's advantages become clearer in repeated evaluations, as shown in the synthetic results in Table II.

Further analysis in Fig. 4 confirms that performance gains are most significant when reactive resources are scarce and proactive budgets are moderate. As reactive capacity increases, the performance gap narrows, but the tri-level framework still offers more efficient allocations. These trends highlight the framework's value in resource-constrained resilience planning. Conversely, increasing proactive investment initially boosts performance but eventually plateaus, aligning with the patterns

observed in the synthetic dataset.

The spatial maps in Fig. 5 highlight how different planning models allocate resilience actions under both mean and adversarial outage scenarios. Fig. 5 (a), the model predicts that worst-case outages are concentrated in inland western counties, such as Berkshire and Hampshire. Fig. 5 (c) displays the actual SAIDI observed during the third storm, which primarily affected coastal regions like Plymouth and Barnstable. This contrast reveals the limitations of planning based solely on average events – such strategies may lead to over-protection in coastal areas while overlooking infrequent but severe risks in inland regions, with less well-developed infrastructure facing severe weather. On the other hand, the conventional robust optimization approach (RO), shown in Fig. 5(d), focuses solely on worst-case disruption, leading to overly conservative proactive investments in the inland areas that ignore coordination with post-event responses. In contrast, our tri-level model proactively protects both high-risk and economically significant counties through coordinated proactive and reactive actions, as shown in Fig. 5 (g). By explicitly considering trade-offs between investment cost and tail-risk exposure, it yields proactive investments whose corresponding worst-case disruption (Fig. 5 (h)) is more equitably distributed across regions with less economic weight. Remaining uncertainties are addressed through targeted reactive deployments (Fig. 5 (i)), ensuring rapid recovery even in less-protected areas. Together, these coordinated actions exemplify a resilient strategy that integrates long-term planning with operational responsiveness.

VII. CONCLUSION

This paper presented a decision framework for proactive grid resilience planning under extreme weather uncertainty. By modeling the problem as a tri-level optimization that links proactive investment, uncertain disruptions, and reactive response, we offered a structured approach to jointly optimize long- and short-term resilience actions. Using spatio-temporal conformal prediction, we constructed adaptive, distribution-free uncertainty sets to address data scarcity and spatial heterogeneity. The reformulated bi-level problem was solved using a scalable Benders decomposition algorithm. Experiments on synthetic and real-world data showed that joint optimization significantly reduces worst-case losses, particularly under tight resource constraints. Our results underscore the importance of anticipatory planning, robust uncertainty modeling, and scalable solvers in building resilient power systems.

REFERENCES

- [1] H. He, S. Huang, Y. Liu, and T. Zhang, "A tri-level optimization model for power grid defense with the consideration of post-allocated dgs against coordinated cyber-physical attacks," *International Journal of Electrical Power and Energy Systems*, vol. 130, p. 106903, 2021. [Online]. Available: <https://www.sciencedirect.com/science/article/pii/S0142061521001435>
- [2] IEEE PES Industry Technical Support Task Force, "The definition and quantification of resilience," IEEE Power & Energy Society, Tech. Rep. PES-TR65, 2018, accessed: April 11, 2025. [Online]. Available: https://resourcecenter.ieee-pes.org/publications/technical-reports/pestr0065_04-18
- [3] Captive.com, *Global Economic Losses \$36 Billion So Far in 2018, over Half Insured*, 2018. [Online]. Available: <https://www.captive.com/news/global-economic-losses-36-billion-so-far-in-2018-over-half-insured>

[4] X. Liu, M. Shahidehpour, Z. Li, X. Liu, Y. Cao, and Z. Bie, "Microgrids for enhancing the power grid resilience in extreme conditions," *IEEE Transactions on Smart Grid*, vol. 8, no. 2, pp. 589–597, 2016.

[5] M. Panteli, D. N. Trakas, P. Mancarella, and N. D. Hatziargyriou, "Power systems resilience assessment: Hardening and smart operational enhancement strategies," *Proceedings of the IEEE*, vol. 105, no. 7, pp. 1202–1213, 2017.

[6] S. Zhu, R. Yao, Y. Xie, F. Qiu, Y. Qiu, and X. Wu, "Quantifying grid resilience against extreme weather using large-scale customer power outage data," *arXiv preprint arXiv:2109.09711*, 2021.

[7] A. M. Stanković, K. L. Tomsovic, F. De Caro, M. Braun, J. H. Chow, N. Čukalevski, I. Dobson, J. Eto, B. Fink, C. Hachmann *et al.*, "Methods for analysis and quantification of power system resilience," *IEEE Transactions on Power Systems*, vol. 38, no. 5, pp. 4774–4787, 2022.

[8] G. Huang, J. Wang, C. Chen, J. Qi, and C. Guo, "Integration of preventive and emergency responses for power grid resilience enhancement," *IEEE Transactions on Power Systems*, vol. 32, no. 6, pp. 4451–4463, 2017.

[9] Y. Lin, B. Chen, J. Wang, and Z. Bie, "A combined repair crew dispatch problem for resilient electric and natural gas system considering reconfiguration and dg islanding," *IEEE Transactions on Power Systems*, vol. 34, no. 4, pp. 2755–2767, 2019.

[10] S. Chen, F. Fioretto, F. Qiu, and S. Zhu, "Global-decision-focused neural odes for proactive grid resilience management," *arXiv preprint arXiv:2502.18321*, 2025.

[11] S. Lei, C. Chen, Y. Li, and Y. Hou, "Resilient disaster recovery logistics of distribution systems: Co-optimize service restoration with repair crew and mobile power source dispatch," *IEEE Transactions on Smart Grid*, vol. 10, no. 6, pp. 6187–6202, 2019.

[12] M. A. Mohamed, T. Chen, W. Su, and T. Jin, "Proactive resilience of power systems against natural disasters: A literature review," *Ieee Access*, vol. 7, pp. 163 778–163 795, 2019.

[13] S. Ma, B. Chen, and Z. Wang, "Resilience enhancement strategy for distribution systems under extreme weather events," *IEEE Transactions on Smart Grid*, vol. 9, no. 2, pp. 1442–1451, 2016.

[14] S. Bao, C. Zhang, M. Ouyang, and L. Miao, "An integrated tri-level model for enhancing the resilience of facilities against intentional attacks," *Annals of Operations Research*, vol. 283, pp. 87–117, 2019.

[15] Y. Wang, A. O. Rousis, and G. Strbac, "A three-level planning model for optimal sizing of networked microgrids considering a trade-off between resilience and cost," *IEEE Transactions on Power Systems*, vol. 36, no. 6, pp. 5657–5669, 2021.

[16] H. Jiang, Y. Xie, and F. Qiu, "Spatio-temporal conformal prediction for power outage data," 2024. [Online]. Available: <https://arxiv.org/abs/2411.17099>

[17] P. D. H. Hines, I. Dobson, and P. Rezaei, "Cascading power outages propagate locally in an influence graph that is not the actual grid topology," *IEEE Transactions on Power Systems*, vol. 32, no. 2, pp. 958–967, 2017.

[18] V. Vovk, A. Gammerman, and G. Shafer, *Algorithmic Learning in a Random World*. Berlin, Heidelberg: Springer-Verlag, 2005.

[19] B. Zeng and L. Zhao, "Solving two-stage robust optimization problems using a column-and-constraint generation method," *Operations Research Letters*, vol. 41, no. 5, pp. 457–461, 2013. [Online]. Available: <https://www.sciencedirect.com/science/article/pii/S0167637713000618>

[20] Y. P. Patel, S. Rayan, and A. Tewari, "Conformal contextual robust optimization," in *International Conference on Artificial Intelligence and Statistics*. PMLR, 2024, pp. 2485–2493.

[21] J. BnnoBRs, "Partitioning procedures for solving mixed-variables programming problems," *Numer. Math.*, vol. 4, no. 1, pp. 238–252, 1962.

[22] "Massachusetts power outages," Massachusetts Emergency Management Agency, Massachusetts, USA, Tech. Rep., 2020.

[23] National Oceanic and Atmospheric Administration, "High-resolution rapid refresh (HRRR) model," <https://rapidrefresh.noaa.gov/hrrr/>, 2024, accessed: 2024-11-11.

[24] D. Bertsimas, D. B. Brown, and C. Caramanis, "Theory and applications of robust optimization," *SIAM Review*, vol. 53, no. 3, pp. 464–501, 2011. [Online]. Available: <https://doi.org/10.1137/080734510>

[25] R. A. Jabr, "Robust transmission network expansion planning with uncertain renewable generation and loads," *IEEE Transactions on Power Systems*, vol. 28, no. 4, pp. 4558–4567, 2013.

[26] A. Ben-Tal, A. Goryashko, E. Guslitzer, and A. Nemirovski, "Adjustable robust solutions of uncertain linear programs," *Mathematical Programming*, vol. 99, no. 2, pp. 351–376, Mar. 2004. [Online]. Available: <https://doi.org/10.1007/s10107-003-0454-y>

[27] D. Bertsimas, L. Na, B. Stellato, and I. Wang, "The benefit of uncertainty coupling in robust and adaptive robust optimization," *INFORMS Journal on Optimization*, Dec. 2024. [Online]. Available: <http://dx.doi.org/10.1287/ijoo.2023.0007>

[28] P. Z. Wang, J. Liang, S. Chen, F. Fioretto, and S. Zhu, "Gen-dfl: Decision-focused generative learning for robust decision making," 2025. [Online]. Available: <https://arxiv.org/abs/2502.05468>

[29] D. Bertsimas and C. Caramanis, "Finite adaptability in multistage linear optimization," *IEEE Transactions on Automatic Control*, vol. 55, no. 12, pp. 2751–2766, 2010.

[30] D. Bertsimas, E. Litvinov, X. A. Sun, J. Zhao, and T. Zheng, "Adaptive robust optimization for the security constrained unit commitment problem," *IEEE Transactions on Power Systems*, vol. 28, no. 1, pp. 52–63, 2013.

[31] B. Zeng, "A practical scheme to compute the pessimistic bilevel optimization problem," *INFORMS Journal on Computing*, vol. 32, no. 4, p. 1128–1142, Oct. 2020.

[32] O. Nohadani and K. Sharma, "Optimization under decision-dependent uncertainty," *SIAM Journal on Optimization*, vol. 28, no. 2, pp. 1773–1795, 2018.

[33] B. Zeng and W. Wang, "Two-stage robust optimization with decision dependent uncertainty," 2022. [Online]. Available: <https://arxiv.org/abs/2203.16484>

[34] G. Brown, M. Carlyle, J. Salmerón, and K. Wood, "Defending critical infrastructure," *Interfaces*, vol. 36, no. 6, pp. 530–544, 2006.

[35] M. Macaš, S. Orlando, S. Costea, P. Novák, O. Chumák, P. Kadera, and P. Kopejko, "Impact of forecasting errors on microgrid optimal power management," in *2020 IEEE International Conference on Environment and Electrical Engineering and 2020 IEEE Industrial and Commercial Power Systems Europe (EEEIC / I&CPS Europe)*, 2020, pp. 1–6.

[36] R. Eskandarpour and A. Khodaei, "Machine learning based power grid outage prediction in response to extreme events," *IEEE Transactions on Power Systems*, vol. 32, no. 4, pp. 3315–3316, 2017.

[37] Y. Wei, C. Ji, F. Galvan, S. Couvillon, G. Orellana, and J. Momoh, "Non-stationary random process for large-scale failure and recovery of power distributions," *arXiv preprint arXiv:1202.4720*, 2012.

[38] F. Li, D. Wang, H. Guo, and J. Zhang, "Distributionally robust optimization for integrated energy system accounting for refinement utilization of hydrogen and ladder-type carbon trading mechanism," *Applied Energy*, vol. 367, p. 123391, 2024. [Online]. Available: <https://www.sciencedirect.com/science/article/pii/S0306261924007748>

[39] W. Zhou, S. Zhu, F. Qiu, and X. Wu, "Hierarchical spatio-temporal uncertainty quantification for distributed energy adoption," *arXiv preprint arXiv:2411.12193*, 2024.

[40] H. Papadopoulos, A. Gammerman, and V. Vovk, "Normalized nonconformity measures for regression conformal prediction," in *Proceedings of the 26th IASTED International Conference on Artificial Intelligence and Applications*, ser. AIA '08. USA: ACTA Press, 2008, p. 64–69.

[41] A. Bellotti, "Constructing normalized nonconformity measures based on maximizing predictive efficiency," in *Proceedings of the Ninth Symposium on Conformal and Probabilistic Prediction and Applications*, ser. Proceedings of Machine Learning Research, A. Gammerman, V. Vovk, Z. Luo, E. Smirnov, and G. Cherubin, Eds., vol. 128. PMLR, 09–11 Sep 2020, pp. 41–54. [Online]. Available: <https://proceedings.mlr.press/v128/bellotti20a.html>

[42] C. Kosma, G. Nikolentzos, G. Panagopoulos, J.-M. Steyaert, and M. Vazirgiannis, "Neural ordinary differential equations for modeling epidemic spreading," *Transactions on Machine Learning Research*, 2023.

[43] "IEEE guide for electric power distribution reliability indices," *IEEE Std 1366-2022 (Revision of IEEE Std 1366-2012)*, pp. 1–44, 2022.

[44] N. Abi-Samra, L. Willis, and M. Moon, *Hardening the System*, 2013. [Online]. Available: <https://www.tdworld.com/vegetation-management/article/20962556/hardening-the-system>

[45] D. Shea, *Hardening the Grid: How States Are Working to Establish a Resilient and Reliable Electric System*, 2018. [Online]. Available: <https://www.ncsl.org/research/energy/hardening-the-grid-how-states-are-working-to-establish-a-resilient-and-reliable-electric-system.aspx>

[46] U.S. Census Bureau, "American community survey 1-year estimates, data profiles: Massachusetts," 2017, accessed: 2025-02-23. [Online]. Available: <https://www.census.gov/acs/www/data/data-tables-and-tools/data-profiles/2017/>

[47] Gurobi Optimization, LLC, "Gurobi Optimizer Reference Manual," 2024. [Online]. Available: <https://www.gurobi.com>

APPENDIX A
INTEGRALITY AND OPTIMALITY OF THE LINEAR
RELAXATION OF THE INNER PROBLEM

The objective in (8) can be rewritten as:

$$\min_{\mathbf{y}} \sum_{i=1}^n \zeta_i (1 - y_i) = \sum_{i=1}^n \zeta_i - \max_{\mathbf{y}} \sum_{i=1}^n \zeta_i y_i \equiv \min_{\mathbf{y}} \sum_{i=1}^n \zeta_i y_i,$$

where the final equivalence follows from the fact that the constant term $\sum_i \zeta_i$ does not affect the optimization. Thus, for fixed proactive decisions \mathbf{x} and outage realizations \mathbf{u} , the inner optimization problem reduces to the following linear program after relaxing the binary variables \mathbf{y} to be continuous in the range $[0, 1]$:

$$\begin{aligned} \min_{\mathbf{y}} \quad & \sum_{i=1}^n \zeta_i y_i \\ \text{s.t.} \quad & \sum_{i=1}^n c_i y_i \leq C, \\ & y_i \in [0, 1], \quad \forall i. \end{aligned} \tag{14}$$

We show the optimal solution to (14) remains binary and optimal after the relaxation under mild assumptions. In particular, the crew assignment recourse action that we considered in the synthetic and real data case studies, with integral crew availability and binary assignments, satisfy such conditions.

Proposition 1. *Let $C \in \mathbb{Z}_+$, and suppose the all cost coefficients $\{\zeta_i\}_{i=1}^n$ that are non-zero are also pairwise distinct. Then every optimal solution \mathbf{y}^* to (14) with the linearly relaxed range $0 \leq y_i \leq 1$ satisfies:*

$$y_i^* \in \{0, 1\} \quad \text{for all } i = 1, \dots, n.$$

Additionally, any such integral solution to the linearly relaxed problem is also optimal for the original problem.

Remark 1. *Intuitively, consider a crew allocation problem. The gradient of the objective function (14) $\partial(\zeta_i y_i) / \partial y_i$ favors assigning full crew resources to the most critical regions. Given the distinct ζ_i for cities with no proactive action, and that crew budget C is multiple of uniform c_i , the solution prioritizes the top-ranked ζ_i until the budget is exhausted, leading to a binary allocation.*

Proof. First, note that the feasible region for the linearly relaxed problem of (14) is a polyhedron:

$$\mathcal{Y} = \left\{ \mathbf{y} \in \mathbb{R}^n : \sum_{i=1}^n y_i \leq C, 0 \leq y_i \leq 1, \forall i \right\}.$$

Since problem (14) is a linear program with a bounded feasible region, an optimal solution is attained at an extreme point or a face of the polyhedron.

It is well known that if the constraint matrix is totally unimodular and the right-hand side is integral, then every extreme point of the feasible region is integral. In our case, the constraints of the relaxed problem can be rewritten in matrix form as:

$$A\mathbf{y} \leq \mathbf{b}, \quad A = \begin{pmatrix} \mathbf{1}^\top \\ I_n \\ -I_n \end{pmatrix}, \quad \mathbf{b} = \begin{pmatrix} C \\ \mathbf{1} \\ \mathbf{0} \end{pmatrix},$$

Since A is totally unimodular and B is an integer, it follows that every extreme point falls in the integral set $\{0, 1\}$ for all i .

Under the mild assumption on the cost coefficients ζ_i being pairwise different for areas that are not proactive protected, thus ruling out ties, every optimal solution to the linear problem is an extreme point and cannot be at any face of polyhedron. Therefore, every optimal solution \mathbf{y}^* to the linear problem must be an extreme point and is hence integral.

To show that these solutions are also optimal for the original integer-constrained problem, notice that the original integer problem's feasible region is contained within that of the relaxed problem, and that any optimal solution from the relaxation that is integral remains feasible. Therefore, the integral solution obtained from the relaxed problem is also optimal for the original integer-constrained problem. \square

APPENDIX B
STRONG DUALITY OF THE RELAXED INNER PROBLEM

The feasible region of (14) is a bounded polyhedron defined by box constraints and a single linear inequality. Since the objective is linear and the feasible region has nonempty relative interior, the problem satisfies Slater's condition, which guarantees strong duality.

Proposition 2. *The linear program in (14) satisfies Slater's condition and therefore admits strong duality.*

Proof. Let $y_i = \min \left(1, C / (2 \sum_{j=1}^n c_j) \right)$ for all i and $y_i \in (0, 1]$. We have

$$\sum_{i=1}^n c_i y_i \leq \frac{C}{2 \sum_{j=1}^n c_j} \sum_{i=1}^n c_i = \frac{C}{2} < C,$$

so this point lies strictly inside the feasible region. Hence, Slater's condition holds and strong duality applies. \square

We now derive the dual of the linear program (14), following standard Lagrangian duality. Let $\lambda \geq 0$ be the dual variable associated with the budget constraint $\sum_i c_i y_i \leq C$, and let $\mu_i \geq 0$ be the dual variables for the upper bound constraints $y_i \leq 1$. We omit explicit dual variables for the lower bounds $y_i \geq 0$, as they are naturally enforced in the non-negativity domain of the primal.

The Lagrangian is:

$$\begin{aligned} \mathcal{L}(\mathbf{y}, \lambda, \boldsymbol{\mu}) &= \sum_{i=1}^n \zeta_i y_i + \lambda \left(\sum_{i=1}^n c_i y_i - C \right) + \sum_{i=1}^n \mu_i (y_i - 1) \\ &= \sum_{i=1}^n y_i (\zeta_i + \lambda c_i + \mu_i) - \lambda C - \sum_{i=1}^n \mu_i. \end{aligned}$$

The dual function is finite only when the coefficients of y_i vanish:

$$\zeta_i + \lambda c_i + \mu_i = 0 \quad \Rightarrow \quad \mu_i = -(\zeta_i + \lambda c_i).$$

Since $\mu_i \geq 0$, this implies:

$$\lambda c_i + \mu_i \geq \zeta_i, \quad \forall i.$$

Substituting into the dual objective yields:

$$\min_{\lambda \geq 0, \mu \geq 0} \lambda C + \sum_{i=1}^n \mu_i, \quad \text{s.t. } \lambda c_i + \mu_i \geq \zeta_i, \quad \forall i.$$

This dual program is used in the bi-level reformulation, replacing the reactive decision layer in the original tri-level model. Its structure preserves linearity and tractability while maintaining robustness through tight worst-case guarantees.

APPENDIX C REFORMULATION VIA KKT CONDITIONS

As an alternative solution strategy to the bi-level formulation in (10), we embed the inner (worst-case) problem into the outer model via the Karush–Kuhn–Tucker (KKT) conditions and solve the resulting single-level formulation with Gurobi [47]. The procedure has following two steps:

1) *KKT Conditions*: The Lagrangian for the inner problem is:

$$\begin{aligned} \mathcal{L}(u, \lambda, \mu, \rho, \sigma, \gamma, \delta_i^{(L)}, \delta_i^{(U)}, \eta^{(L)}, \eta^{(U)}) = & \\ & - \sum_{i=1}^n h_i u_i (1 - x_i) + \lambda C + \sum_{i=1}^n \mu_i \\ & + \sum_{i=1}^n \rho_i (h_i u_i (1 - x_i) - \lambda - \mu_i) \\ & + \sum_{i=1}^n \sigma_i (-\mu_i) + \gamma (-\lambda) \\ & + \sum_{i=1}^n \delta_i^{(L)} (L_i - u_i) + \sum_{i=1}^n \delta_i^{(U)} (u_i - T_i) \\ & + \eta^{(L)} (\hat{L}_0(\mathbf{w}) - \sum_{i=1}^n u_i) + \eta^{(U)} (\sum_{i=1}^n u_i - \hat{T}_0(\mathbf{w})). \end{aligned} \quad (15)$$

where $\rho_i, \sigma_i, \gamma, \delta_i^{(L)}, \delta_i^{(U)}, \eta^{(L)}, \eta^{(U)}$ are Lagrange multipliers.

The primal feasibility conditions enforce:

$$\lambda + \mu_i - h_i u_i (1 - x_i) \geq 0, \quad \forall i, \quad (16)$$

$$L_i \leq u_i \leq T_i, \quad \forall i, \quad (17)$$

$$\hat{L}_0(\mathbf{w}) \leq \sum_{i=1}^n u_i \leq \hat{T}_0(\mathbf{w}). \quad (18)$$

The dual feasibility constraints require:

$$\begin{aligned} \rho_i \geq 0, \quad \sigma_i \geq 0, \quad \gamma \geq 0, \\ \delta_i^{(L)} \geq 0, \quad \delta_i^{(U)} \geq 0, \quad \eta^{(L)} \geq 0, \quad \eta^{(U)} \geq 0. \end{aligned} \quad (19)$$

The stationarity conditions are:

$$\frac{\partial \mathcal{L}}{\partial u_i} = -h_i (1 - x_i) + \rho_i h_i (1 - x_i) - \delta_i^{(L)} \quad (20)$$

$$+ \delta_i^{(U)} - \eta^{(L)} + \eta^{(U)} = 0, \quad \forall i, \quad (21)$$

$$\frac{\partial \mathcal{L}}{\partial \lambda} = B - \sum_{i=1}^n \rho_i - \gamma = 0, \quad (22)$$

$$\frac{\partial \mathcal{L}}{\partial \mu_i} = 1 - \rho_i - \sigma_i = 0, \quad \forall i. \quad (23)$$

The complementary slackness conditions enforce:

$$\rho_i (\lambda + \mu_i - h_i u_i (1 - x_i)) = 0, \quad \forall i, \quad (24)$$

$$\sigma_i \mu_i = 0, \quad \forall i, \quad (25)$$

$$\gamma \lambda = 0, \quad (26)$$

$$\delta_i^{(L)} (u_i - L_i) = 0, \quad \forall i, \quad (27)$$

$$\delta_i^{(U)} (T_i - u_i) = 0, \quad \forall i, \quad (28)$$

$$\eta^{(L)} \left(\sum_{i=1}^n u_i - \hat{L}_0(\mathbf{w}) \right) = 0, \quad (29)$$

$$\eta^{(U)} \left(\hat{T}_0(\mathbf{w}) - \sum_{i=1}^n u_i \right) = 0, \quad (30)$$

This reformulation ensures the solution satisfies all primal, dual, and optimality constraints while maintaining clear notation distinctions.

Plugging the middle-layer KKT solutions into the upper-layer problem, we obtain the following single-layer formulation:

$$\begin{aligned} \min_{\mathbf{x}} \sum_i h_i u_i (1 - x_i) - \left(\lambda C + \sum_{i=1}^n \mu_i \right) \\ \text{s.t. } \sum_{i=1}^n x_i \leq B, \quad x_i \in \{0, 1\}, \quad u_i \geq 0. \end{aligned} \quad (31)$$

and constraints (16) - (30).

2) *Linearization with Big-M*: To solve this reformulated single-layer problem using commercial solvers such as Gurobi, all KKT constraints must be linear. Therefore, we apply the Big-M method to linearize (24) with following inequalities:

$$\lambda + \mu_i - h_i u_i (1 - x_i) \leq M(1 - z_i), \quad (32)$$

$$\rho_i \leq z_i M, \quad (33)$$

where M is a sufficiently large constant, and the binary variable z_i ensures either $z_i = 0$ and $\rho_i = 0$, or $z_i = 1$ and $\lambda + \mu_i - h_i u_i (1 - x_i) = 0$.

The resulting single-level mixed-integer linear programme (MILP) captures all primal, dual, and optimality conditions of the original bi-level problem (10) and can be solved directly with Gurobi [47] with Big-M linearization.

APPENDIX D ADDITIONAL RESULTS

A. Conformal Prediction Performances

To assess the effectiveness of the normalized conformal prediction (NCP) model for outage estimation, we compare it with traditional conformal prediction (CP) and empirical upper bound estimates (Emp), which serve as a baseline.

Table IV reports the performance of the proposed Spatio-Temporal Normalized Conformal Prediction (NCP) model for constructing uncertainty intervals. Compared to empirical confidence intervals based on historical normality assumptions, NCP achieves perfect coverage with competitive efficiency, producing narrower average interval widths and significantly

TABLE IV
OUT-OF-SAMPLE PERFORMANCE METRICS FOR CONFORMAL PREDICTION INTERVALS ON SYNTHETIC DATASET

Level	Pred \hat{f}	Coverage		Efficiency (Avg. Interval Width)	MSE	
		(%)	(Avg. Interval Width)			
County ($\alpha = 0.99$)	Emp	97.75	10.8	8.6	2.48	
	CP	99.0	9.8	2.48		
	NCP	99.5	8.4			
Aggregated ($\alpha = 0.5$)	Emp	40.0	12.1	70.7	490.0	
	CP	50.0	37.5	490.0		
	NCP	50.0	37.5			

* Empirical mean and confidence interval estimated from historical data assuming normality.

TABLE V
OUT-OF-SAMPLE PERFORMANCE METRICS FOR 90% CONFORMAL PREDICTION INTERVALS ON MA DATASET

Level	Pred \hat{f}	Coverage		Efficiency (Avg. Interval Width)	MSE	
		(%)	(Avg. Interval Width)			
County	Emp	90.9	104.9	1412.3	557.4	
	CP	90.9	57.5	557.4		
	NCP	81.8	255.3			

* Empirical mean and confidence interval estimated from historical data assuming normality.

lower mean squared error (MSE). These improvements reflect NCP's ability to capture heteroskedastic and region-specific uncertainties more effectively than conventional methods. This highlights the importance of integrating data-driven uncertainty models within resilience-focused optimization frameworks.

B. Subsampling Study for Solution Verification and Efficiency Comparison

To further validate the scalability of the proposed Benders decomposition approach, we conduct a subsampling study using data from 44 counties in Florida affected by Hurricane Ian in 2022. Florida is selected instead of Massachusetts because its larger number of counties enables a more meaningful evaluation of scalability in real-world data. For benchmarking both the quality of the solution and the computational efficiency, we implement a brute-force solution solving (10) by traversing all possible combinations of proactive decision in the outer layer, in addition to applying the KKT approach (see Appendix C).

Fig. 6 compares the computation time and relative solution differences between Benders and brute-force methods across different problem sizes. Results are averaged over four random subsamples with standard error (SE) reported. The findings confirm that the Benders decomposition approach achieves optimal solutions with significantly reduced computational time compared to brute-force and KKT methods, especially as the problem size increases.

APPENDIX E MIDDLE LAYER RELAXATION

In this section, we show a special case to the middle layer of (1) when the local conformal predicted bounds are not

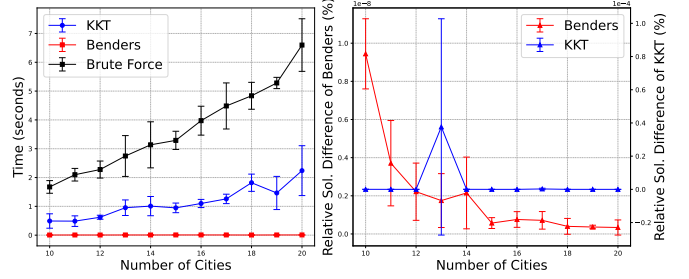


Fig. 6. Comparison of computation time and relative objective solution difference compared to Brute Force method with varying problem size. Results and standard error (SE) are based on four randomly subsampled cities in Florida during the outages caused by Hurricane Ian.

binding, the problem becomes a simple disruption budget allocation problem for the natural attacker, therefore result in a intuitive solution that carry good intuition for understanding the dynamics of the worst-case attack. We note that while this condition seems hard to obtain, the similarity of the results of adversarial attack without (5) and that with full uncertainty set (7) in Table II and Table III shows that this is a good approximation to the original problem.

Proposition 3. Order the economic weights so that

$$h_{(1)} \leq h_{(2)} \leq \cdots \leq h_{(n)}.$$

Then the attacker's optimal allocation \mathbf{u}^* has support on the $C + 1$ smallest h -indices:

$$u_{(i)}^* = \begin{cases} \frac{T_0/h_{(i)}}{\sum_{j=1}^{C+1} \frac{1}{h_{(j)}}}, & i = 1, \dots, C + 1, \\ 0, & i = C + 2, \dots, n, \end{cases}$$

and the defender uses its C repairs on the C largest products $h_{(i)} u_{(i)}^*$.

Proof. For any fixed \mathbf{u} , the defender sets $y_i = 1$ on the C indices with largest $h_i u_i$, removing those terms from the sum. Thus the attacker solves

$$\max_{\sum_i u_i = T_0} \min_{\substack{S \subseteq \{1, \dots, n\} \\ |S|=C}} \sum_{i \notin S} h_i u_i.$$

By symmetry and convexity, the optimum equalizes the surviving $h_i u_i$ values over $n - C$ indices. To prevent the defender from eliminating all budget, the attacker restricts to the $C + 1$ smallest h , then distributes T_0 across those indices in proportion to $1/h_{(i)}$. Enforcing $\sum_{i=1}^{C+1} u_{(i)} = T_0$ and $h_{(1)} u_{(1)} = \dots = h_{(C+1)} u_{(C+1)}$ yields the closed-form \mathbf{u}^* in the proposition. \square

Remark 2. Intuitively, this proposition shows the adversary allocates its disruption budget, T_0 , inversely to the cost coefficients h_i (e.g. population) among the $C+1$ least costly regions so that reactive repairs can eliminate at most C of them. While we ignore the outer layer for simplicity, we can easily apply the proposition to the non-proactively protected counties, resulting in same scheme. Figure 5 visualizes this intuition: the worst-case attack for both strategies concentrates on low-populated counties that are not proactively protected, since we have set economic weights equal to the customer count $h_i = N_i$.

APPENDIX F BASELINE FORMULATION

We compare our trilevel approach with the following alternative optimization strategies:

a) *One Stage Optimization*: This formulation makes proactive decisions \mathbf{x} to minimize the expected economic loss:

$$\min_{\mathbf{x} \in \mathcal{X}} \sum_{i=1}^n h_i \hat{u}_i (1 - x_i),$$

where \hat{u}_i represents the predicted outage level for region i . Reactive decisions \mathbf{y} are then made optimally, based on the actual outcomes of \mathbf{u} after the proactive actions \mathbf{x} are determined.

b) *One Stage Worst-Case Optimization*: In this approach, proactive actions \mathbf{x} are chosen to minimize the worst-case economic loss:

$$\min_{\mathbf{x} \in \mathcal{X}} \max_{\mathbf{u} \in \mathcal{U}} \sum_{i=1}^n h_i u_i (1 - x_i).$$

c) *Two Stage Optimization*: Next, we build upon the *mean-case* single-level formulation by incorporating reactive decisions \mathbf{y} alongside proactive measures:

$$\min_{\mathbf{x} \in \mathcal{X}, \mathbf{y} \in \mathcal{Y}} \sum_{i=1}^n h_i \hat{u}_i (1 - x_i) (1 - y_i).$$

d) *Two Stage Worst-case Optimization*: Finally, we extend the *worst-case* optimization approach to include both proactive and reactive decisions to minimize the worst-case economic loss:

$$\min_{\mathbf{x} \in \mathcal{X}, \mathbf{y} \in \mathcal{Y}} \max_{\mathbf{u} \in \mathcal{U}} \sum_{i=1}^n h_i u_i (1 - x_i) (1 - y_i).$$

APPENDIX G SYNTHETIC EXPERIMENT SETUP

This section outlines the procedure used to generate synthetic outage trajectories for evaluating the proposed tri-level framework. We simulate disruptions using a spatio-temporal compartmental model that reflects the spread and resolution of outages across regions, driven by synthetic weather conditions and population characteristics.

Each region i follows an independent SIR-style (Susceptible–Infected–Recovered) dynamic [6], [37], where the number of disrupted customers evolves over time in response to localized weather conditions. The compartments are defined as follows:

- $S_i(t)$: number of unaffected (susceptible) customers at time t ,
- $Y_i(t)$: number of disrupted (infected) customers at time t ,
- $R_i(t)$: number of recovered customers at time t ,

with total population $N_i = S_i(t) + Y_i(t) + R_i(t)$ conserved over time.

The evolution of the outage process is governed by the following system of ordinary differential equations:

$$\frac{dS_i(t)}{dt} = -\beta_i \cdot \frac{S_i(t) \cdot Y_i(t)}{N_i}, \quad (34)$$

$$\frac{dY_i(t)}{dt} = \beta_i \cdot \frac{S_i(t) \cdot Y_i(t)}{N_i} - \gamma_i Y_i(t), \quad (35)$$

$$\frac{dR_i(t)}{dt} = \gamma_i Y_i(t), \quad (36)$$

where β_i is the disruption rate and γ_i is the recovery rate.

We parameterize the disruption rate β_i as a linear function of weather variables and set γ_i to be a constant:

$$\begin{aligned} \beta_i &= 0.3 + 0.01(\text{Temp}_i - 20) + 0.005(\text{Wind}_i - 10) \\ &\quad - 0.005(\text{Hum}_i - 0.5), \\ \gamma_i &= 0.1. \end{aligned} \quad (37)$$

Let $(p_i, q_i) \in [0, 1]^2$ be the normalized spatial coordinates of region i . The temperature, wind speed, and humidity at each location are defined as:

$$\begin{aligned} \text{Temp}_i &= 20 + 5 \cdot \sin(2\pi p_i) \cdot \cos(2\pi q_i), \\ \text{Wind}_i &= 10 + 3 \cdot \cos(2\pi p_i) \cdot \sin(2\pi q_i), \\ \text{Hum}_i &= 0.5 + 0.1 \cdot \sin(2\pi p_i) \cdot \sin(2\pi q_i). \end{aligned}$$

These functional forms yield spatially correlated weather patterns, ensuring that nearby regions experience similar meteorological conditions, mimicking real-world climate systems (see Fig. 7).

To numerically solve the ODEs, we apply the Euler method with a fixed time step $\Delta t = 0.1$, simulating until all disruptions are resolved (i.e., $Y_i(t)$ converges to zero). The total duration of outage in region i is then used to compute the SAIDI index:

$$u_i = \frac{1}{N_i} \int_0^{\infty} Y_i(t) dt.$$

In practice, the integral is approximated via numerical summation over discrete time steps:

$$u_i \approx \frac{1}{N_i} \sum_{t=0}^{T_{\max}} Y_i(t) \cdot \Delta t.$$

To reflect measurement noise or modeling uncertainty, we perturb the SAIDI values with heteroskedastic Gaussian noise:

$$\tilde{u}_i = u_i + \varepsilon_i, \quad \varepsilon_i \sim \mathcal{N}\left(0, \frac{\sigma^2}{N_i^2}\right),$$

where σ is a global noise parameter. This formulation captures the intuition that more populous regions (higher N_i) tend to have lower relative variance in aggregate outage observations, aligning with properties observed in real-world data.

We generate 200 synthetic disruption events and reserve 40 for testing. All evaluation metrics are reported as averages over the test set.

APPENDIX H CASE STUDY SETUP

This section provides implementation details for the semi-synthetic case study in Section VI. We combine real outage data from 14 Massachusetts counties during the March 2018 Nor'easter events [22] with simulated cost parameters. Meteorological features (wind, temperature, pressure) are drawn from NOAA's HRRR model [23], and socioeconomic indicators (income, age, food stamps, commute time, etc.) from the

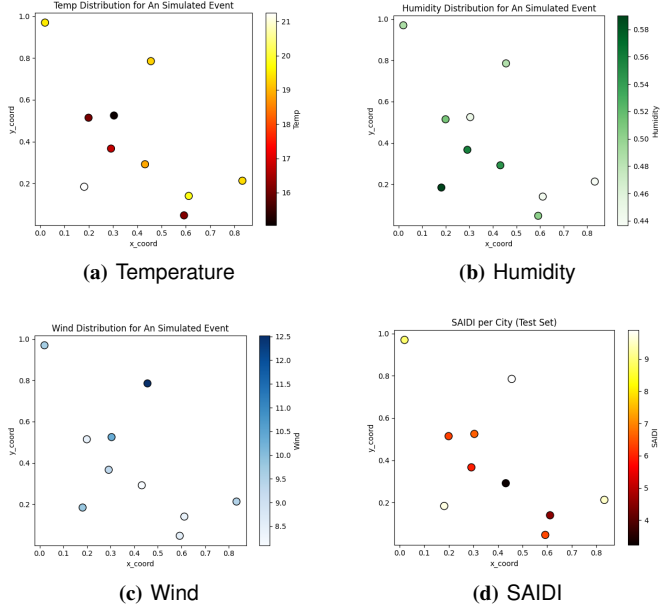


Fig. 7. Spatial distribution of Outage Magnitudes and Weather Features for Ten Cities in the Synthetic Dataset

U.S. Census [46]. The first two storms are used for training conformal bounds; the third serves as the evaluation set.

We simulate proactive undergrounding decisions under a fixed budget $B = 1000$, where each county's cost b_i is randomly sampled from $\text{Unif}(100, 1000)$ to reflect spatial cost heterogeneity. Reactive recovery is modeled using crew dispatch decisions y_{ij} with a capacity limit of $C = 3$, allowing at most one crew per county.

To estimate the local bounds (5) for each counties, we use both traditional Conformal Prediction (CP) and our Normalized Conformal Prediction (NCP) approach. Both models use the same neural network backbone with two hidden layers (64 and 32 units, ReLU activation), predicting SAIDI and residuals from weather and demographic inputs.

Due to the limited number of events, we estimate the lower and upper bounds of total disruption across all regions—denoted $\widehat{L}_0(\cdot)$ and $\widehat{T}_0(\cdot)$ —by taking the empirical mean minus and plus one standard deviation, each computed from the first two outages.